

TE and TM beam decomposition of time-harmonic electromagnetic waves

Timor Melamed

Department of Electrical and Computer Engineering, Ben-Gurion University of the Negev,
Beer Sheva 84105, Israel (timormel@ee.bgu.ac.il)

Received December 20, 2010; accepted January 18, 2011;
posted January 19, 2011 (Doc. ID 139828); published February 25, 2011

The present contribution is concerned with applying beam-type expansion to planar aperture time-harmonic electromagnetic field distribution in which the propagating elements, the electromagnetic beam-type wave objects, are decomposed into transverse electric (TE) and transverse magnetic (TM) field constituents. This procedure is essential for applying Maxwell's boundary conditions for solving different scattering problems. The propagating field is described as a discrete superposition of tilted and shifted TE and TM electromagnetic beams over the frame-based spatial-directional expansion lattice. These vector wave objects are evaluated either by applying differential operators to scalar beam propagators, or by using plane-wave spectral representations. Explicit asymptotic expressions for scalar, as well as for electromagnetic, Gaussian beam propagators are presented as well. © 2011 Optical Society of America

OCIS codes: 350.5500, 070.2580, 080.2720, 260.1960.

1. INTRODUCTION

The directional and spatial localization of beam-type (phase-space) spectral representations make these schemes highly suitable for propagation in complex environments [1–6]. In these expansion schemes, the propagating elements are Gaussian beams, which have been termed phase-space (spectral) Green's functions [7,8]. Such *scalar* propagators have been obtained in homogeneous [1–4], anisotropic [9–11], dispersive [12–14], and inhomogeneous media [15–17]. Several *electromagnetic* beam scattering and diffraction problems have been solved for rough surface scattering [18,19], dielectric interfaces [20], surfaces of perfectly electric conductor [21,22], stratified [23] and negative isotropic media [24], and more. Recently, novel time-harmonic [25–27] beam-type wave objects were obtained by applying a nonorthogonal coordinate system that is *a priori* matched to localized aperture field distributions. These wave objects, which were termed tilted Gaussian/pulsed beams, are suitable for planar beam-type expansions and exhibit enhanced accuracy over the commonly used paraxial solutions.

Exact continuous beam decompositions of scalar time-harmonic fields have been introduced in [1] and in [2] for a two-dimensional (2D) and a three-dimensional case, respectively. These representations are highly overcomplete and, therefore, may be *a priori* discretized. A discrete field expansion, the frame-based beam summation method [4], overcomes the inherent problems of Gabor representation [28] by introducing overcompleteness into the beam-type spectral representations. In this representation, the field is described by a discrete superposition of beams, which emanate from a discrete set of points in the aperture and in a discrete set of directions. The excitation amplitudes of the beam propagators are samples of the local (windowed) spectrum of the aperture field distribution over the frame spatial-directional lattice.

In [29–31], Gaussian beams have been used for the analysis of large reflector antennas, in which the expansion coefficients

are obtained by numerically matching Gaussian beams to the far zone field of the feed antenna. These methods, which employ only propagating spectrum information and do not match the beam spectra to the evanescent spectral constituents, cannot be applied for near-field analysis or in exact field calculations.

Recently, the scalar field expansion scheme was extended to include *electromagnetic* (EM) field expansion in which an exact frame-based expansion of planar aperture time-harmonic EM field was introduced [32]. The propagating EM field is described as a discrete superposition of tilted and shifted EM Gaussian beams over the frame lattice. The propagating wave objects are localized solutions of Maxwell's equations that carry a Gaussian decay away from the beams' axes. Nevertheless, these solutions include both transverse electric (TE) and transverse magnetic (TM) wave polarizations, and thus are not suitable for applying Maxwell's boundary conditions for solving different scattering problems. In the present paper, the EM field is *a priori* decomposed into the two polarizations by processing (expanding) the transverse field components into novel TE and TM EM beam-type wave objects.

The paper outline is as follows: In Section 2, a brief description of TE and TM plane-wave decomposition of aperture fields is given. The scalar frame-based beam decomposition is given in Section 3 with the necessary extensions, which are required for the vectorial representation. In Section 4, the EM field is decomposed into TE/TM EM beams over the frame spatial-directional lattice. The special case of Gaussian windows is discussed in Section 5, as is the corresponding asymptotic expressions for the beam propagators. Finally, a numerical example is given in Section 6.

2. PLANE-WAVE DECOMPOSITION

We are concerned with obtaining a discrete exact TE and TM (with respect to constant z planes) spectral representation for

the time-harmonic EM field in $z \geq 0$ due to sources in $z < 0$, given the transverse electric field components over the $z = 0$ plane:

$$\mathbf{E}_0(\mathbf{r}_t) = E_x(\mathbf{r}_t)\hat{\mathbf{x}} + E_y(\mathbf{r}_t)\hat{\mathbf{y}}, \quad (1)$$

where $\hat{\mathbf{x}}$ and $\hat{\mathbf{y}}$ are the conventional Cartesian unit vectors and $\mathbf{r}_t = (x, y)$ denotes the *transverse* coordinates. We use the conventional Cartesian coordinate system in which the configuration space is described by $\mathbf{r} = (x, y, z)$. The propagation medium is homogeneous with ϵ_0 and μ_0 denoting the free space permittivity and permeability, respectively, and a time dependence of $\exp(j\omega t)$ is assumed for all field quantities. The *plane-wave spectrum* of the aperture field transverse components, which is denoted here by

$$\tilde{\mathbf{E}}_0(\mathbf{k}_t) = \tilde{E}_x(\mathbf{k}_t)\hat{\mathbf{x}} + \tilde{E}_y(\mathbf{k}_t)\hat{\mathbf{y}}, \quad (2)$$

is given by the spatial Fourier transform

$$\tilde{\mathbf{E}}_0(\mathbf{k}_t) = \int d^2r_t \mathbf{E}_0(\mathbf{r}_t) \exp(j\mathbf{k}_t \cdot \mathbf{r}_t), \quad (3)$$

where $\mathbf{k}_t = (k_x, k_y)$ is used to denote *transverse* spectral wavenumbers, so that the exponent in Eq. (3) reads $\mathbf{k}_t \cdot \mathbf{r}_t = k_x x + k_y y$. Throughout this work, all integral limits of $-\infty$ to ∞ are omitted and plane-wave (wavenumber) spectral distributions, such as $\tilde{\mathbf{E}}_0(\mathbf{k}_t)$, are denoted by an over tilde (\sim). By applying a standard plane-wave analysis, which follows directly from Gauss law, the longitudinal spectrum, \tilde{E}_z , is given by

$$\tilde{E}_z(\mathbf{k}_t) = -(k_x \tilde{E}_x + k_y \tilde{E}_y)/k_z, \quad (4)$$

where $k_z = \sqrt{k^2 - k_x^2 - k_y^2}$, with $\text{Im}k_z \leq 0$ and $\text{Re}k_z \geq 0$ is the longitudinal wavenumber. Here $k = \omega/c$ denotes the medium's wavenumber with c denoting the speed of light in free space. Thus, the electric field in $z \geq 0$ is given by the plane-wave superposition:

$$\mathbf{E}(\mathbf{r}, t) = \frac{1}{(2\pi)^2} \int d^2k_t \tilde{\mathbf{E}}(\mathbf{k}_t) \exp(-j\mathbf{k} \cdot \mathbf{r}), \quad (5)$$

where $\mathbf{k} = (k_x, k_y, k_z)$, $d^2k_t = dk_x dk_y$, and $\tilde{\mathbf{E}}(\mathbf{k}_t)$ is the aperture spectral distribution on $z = 0$ plane, i.e.,

$$\tilde{\mathbf{E}}(\mathbf{k}_t) = \tilde{\mathbf{E}}_0(\mathbf{k}_t) + \hat{\mathbf{z}}\tilde{E}_z(\mathbf{k}_t), \quad (6)$$

where \tilde{E}_z is given in Eq. (4).

The plane-wave representation in Eq. (5) describes the electric field in terms of EM plane-wave propagators, which emanate from the $z = 0$ plane in the direction of unit vectors $\hat{\mathbf{k}} = \mathbf{k}/k$. This representation can be rewritten as a superposition of TE and TM plane-waves spectra with respect to planes of constant z [33,34]. To that extent, two spectral unit vectors are defined for a given spectral plane wave. $\hat{\mathbf{n}}(\mathbf{k}_t)$ denotes the *normal* to the so-called plane of incidence, whereas the *tangent* unit vector is denoted by $\hat{\mathbf{t}}(\mathbf{k}_t) = \hat{\mathbf{k}} \times \hat{\mathbf{n}}$. Thus, for a given \mathbf{k}_t ,

$$\hat{\mathbf{n}}(\mathbf{k}_t) = \frac{1}{k_t}(k_y \hat{\mathbf{x}} - k_x \hat{\mathbf{y}}), \quad \hat{\mathbf{t}}(\mathbf{k}_t) = \frac{k_z}{k k_t}(k_x \hat{\mathbf{x}} + k_y \hat{\mathbf{y}}) - \frac{k_t}{k} \hat{\mathbf{z}}, \quad (7)$$

where $k_t = \sqrt{k_x^2 + k_y^2}$. Note that both unit vectors are normal to the spectral plane-wave direction, i.e., $\hat{\mathbf{n}} \cdot \hat{\mathbf{k}} = \hat{\mathbf{t}} \cdot \hat{\mathbf{k}} = 0$.

The TE and TM spectral distributions are obtained by projecting the aperture spectral distribution, $\tilde{\mathbf{E}}(\mathbf{k}_t)$, on the unit vectors in Eq. (7), so that the aperture spectral distribution in Eq. (6) is recast as a sum of the TE and TM spectral distributions:

$$\tilde{\mathbf{E}}(\mathbf{k}_t) = \tilde{E}^{\text{TE}}(\mathbf{k}_t)\hat{\mathbf{n}}(\mathbf{k}_t) + \tilde{E}^{\text{TM}}(\mathbf{k}_t)\hat{\mathbf{t}}(\mathbf{k}_t), \quad (8)$$

where

$$\begin{aligned} \tilde{E}^{\text{TE}}(\mathbf{k}_t) &= \tilde{\mathbf{E}}(\mathbf{k}_t) \cdot \hat{\mathbf{n}}(\mathbf{k}_t) = \frac{1}{k_t}(k_y \tilde{E}_x - k_x \tilde{E}_y), \\ \tilde{E}^{\text{TM}}(\mathbf{k}_t) &= \tilde{\mathbf{E}}(\mathbf{k}_t) \cdot \hat{\mathbf{t}}(\mathbf{k}_t) = \frac{k}{k_z k_t}(k_x \tilde{E}_x + k_y \tilde{E}_y). \end{aligned} \quad (9)$$

By using Eqs. (7) and (9) with Eq. (8) in Eq. (5), we decompose the electric field:

$$\mathbf{E}(\mathbf{r}, t) = \mathbf{E}^{\text{TE}}(\mathbf{r}, t) + \mathbf{E}^{\text{TM}}(\mathbf{r}, t), \quad (10)$$

where

$$\begin{aligned} \mathbf{E}^{\text{TE}}(\mathbf{r}, t) &= \frac{1}{(2\pi)^2} \int d^2k_t \tilde{E}^{\text{TE}}(\mathbf{k}_t)\hat{\mathbf{n}}(\mathbf{k}_t) \exp(-j\mathbf{k} \cdot \mathbf{r}), \\ \mathbf{E}^{\text{TM}}(\mathbf{r}, t) &= \frac{1}{(2\pi)^2} \int d^2k_t \tilde{E}^{\text{TM}}(\mathbf{k}_t)\hat{\mathbf{t}}(\mathbf{k}_t) \exp(-j\mathbf{k} \cdot \mathbf{r}). \end{aligned} \quad (11)$$

Note that, by summing over the spectral representations of $\mathbf{E}^{\text{TE}}(\mathbf{r}, t)$ and $\mathbf{E}^{\text{TM}}(\mathbf{r}, t)$ in Eq. (11), we obtain the plane-wave representation in Eq. (5).

3. SCALAR FRAME-BASED BEAM DECOMPOSITION

In order to establish the TE/TM EM frame-based beam decomposition, we shall briefly review here the main results of the scalar beam expansion that were introduced in [4] along with essential extensions that are required for the TE/TM decomposition in Section 4. The frame-based beam summation is constructed over the discrete frame spatial-directional lattice

$$(\bar{x}, \bar{y}, \bar{k}_x, \bar{k}_y) = (N_x \Delta \bar{x}, N_y \Delta \bar{y}, N_{k_x} \Delta \bar{k}_x, N_{k_y} \Delta \bar{k}_y), \quad (12)$$

where $(\Delta \bar{x}, \Delta \bar{y})$ and $(\Delta \bar{k}_x, \Delta \bar{k}_y)$ are the unit-cell dimensions in the (x, y) and (k_x, k_y) coordinates, respectively, and the index $N = (N_x, N_y, N_{k_x}, N_{k_y})$ is used to tag the lattice points (see Fig. 1). These unit-cell dimensions satisfy

$$\Delta \bar{x} \Delta \bar{k}_x = 2\pi\nu_x, \quad \Delta \bar{y} \Delta \bar{k}_y = 2\pi\nu_y, \quad (13)$$

where $0 \leq \nu_{x,y} \leq 1$ are the overcompleteness parameters in the x or y axes. The lattice is overcomplete for $\nu_{x,y} < 1$, critically complete in the Gabor limit $\nu_{x,y} \uparrow 1$ [28,35,36], and, for $\nu_{x,y} \downarrow 0$, the discrete parameterization attains the continuity limit as in [1,2].

Upon setting the frame lattice, one proceeds by choosing a proper synthesis ("mother") window, $\psi(\mathbf{r}_t)$, and constructs

the windowed Fourier transform frame in the space of all the square integrable functions $\mathbb{L}_2(\mathbb{R})$ on the frame lattice. The 2D synthesis window, $\psi(\mathbf{r}_t)$, is obtained by a Cartesian multiplication of two one-dimensional windows, each yielding a proper frame in $\mathbb{L}_2(\mathbb{R})$. The frame representation of some aperture scalar field distribution over $z = 0$ plane, which is denoted here by $u_0(\mathbf{r}_t)$, is given by

$$u_0(\mathbf{r}_t) = \sum_N a_N \psi_N(\mathbf{r}_t), \quad (14)$$

where the expansion frame set, $\psi_N(\mathbf{r}_t)$, is obtained from the synthesis window, $\psi(\mathbf{r}_t)$, via

$$\psi_N(\mathbf{r}_t) = \psi(\mathbf{r}_t - \bar{\mathbf{r}}_t) \exp[-j\bar{\mathbf{k}}_t \cdot (\mathbf{r}_t - \bar{\mathbf{r}}_t)], \quad (15)$$

where $\bar{\mathbf{r}}_t = (\bar{x}, \bar{y})$ and $\bar{\mathbf{k}}_t = (\bar{k}_x, \bar{k}_y)$ are used to denote the frame lattice points in Eq. (12), and the expansion coefficients, a_N , are given by the inner product of the aperture distribution with the so-called analysis (“dual”) window, $\varphi(\mathbf{r}_t)$, namely,

$$a_N = \int d^2 r_t u_0(\mathbf{r}_t) \varphi_N^*(\mathbf{r}_t), \quad (16)$$

where, similarly to (15),

$$\varphi_N(\mathbf{r}_t) = \varphi(\mathbf{r}_t - \bar{\mathbf{r}}_t) \exp[-j\bar{\mathbf{k}}_t \cdot (\mathbf{r}_t - \bar{\mathbf{r}}_t)]. \quad (17)$$

The analysis window, $\varphi(\mathbf{r}_t)$, can be evaluated by several ways that are listed in [4] [see also Eq. (39)].

The scalar field in $z > 0$, due to sources in $z < 0$, is obtained by propagating each $\psi_N(\mathbf{r}_t)$ window element in summation (14), into $z > 0$ half-space. Therefore, the frame-based representation of the field in $z \geq 0$ is given by

$$u(\mathbf{r}, t) = \sum_N a_N P_N(\mathbf{r}, t), \quad (18)$$

where each beam propagator, $P_N(\mathbf{r}, t)$, satisfies the scalar Helmholtz equation:

$$(\nabla^2 + k^2)P_N(\mathbf{r}, t) = 0. \quad (19)$$

The beam propagator can be evaluated in several ways, such as Green’s function (Kirchhoff’s) integration or by a plane-wave spectral decomposition of the form

$$P_N(\mathbf{r}, t) = \frac{1}{(2\pi)^2} \int d^2 k_t \tilde{\psi}_N(\mathbf{k}_t) \exp(-j\mathbf{k} \cdot \mathbf{r}), \quad (20)$$

where

$$\tilde{\psi}_N(\mathbf{k}_t) = \tilde{\psi}(\mathbf{k}_t - \bar{\mathbf{k}}_t) \exp(j\bar{\mathbf{k}}_t \cdot \bar{\mathbf{r}}_t), \quad (21)$$

with $\tilde{\psi}(\mathbf{k}_t)$ denoting the plane-wave spectral distribution of $\psi(\mathbf{r}_t)$ as in Eq. (22). The spectral representation in Eq. (18) describes the field as a discrete superposition of beam-type wave objects, that emanate from points (\bar{x}, \bar{y}) on the frame lattice, in a discrete set of directions that are determined by the spectral wavenumbers (\bar{k}_x, \bar{k}_y) over the frame lattice (see Fig. 1). In Section 4, a vectorial EM analogue of this re-

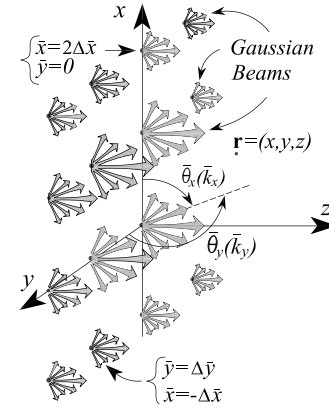


Fig. 1. Discrete frame lattice. The fields in $z \geq 0$ are evaluated by a superposition of tilted and shifted beams that originate from the aperture distribution plane over the discrete frame spatial-directional lattice in Eq. (12). Each beam propagator emanates from a lattice point $(\bar{x}, \bar{y}) = (N_x \Delta \bar{x}, N_y \Delta \bar{y})$ and in a direction of $(\bar{\theta}_x, \bar{\theta}_y) = \cos^{-1}[(\bar{k}_x, \bar{k}_y)/k]$ with respect to the corresponding axis.

presentation is obtained, in which the electric and magnetic fields are described by a superposition of TE and TM *EM beam propagators*.

In order to obtain a discrete *vectorial* frame-based representation, we shall relate the plane-wave spectrum of the aperture field distribution to its frame representation in Eq. (14). The (scalar) *plane-wave spectrum*, $\tilde{u}_0(\mathbf{k}_t)$, is obtained by applying the Fourier operator in Eq. (3) to $u_0(\mathbf{r}_t)$, i.e.,

$$\tilde{u}_0(\mathbf{k}_t) = \int d^2 r_t u_0(\mathbf{r}_t) \exp(j\mathbf{k}_t \cdot \mathbf{r}_t). \quad (22)$$

By inserting Eq. (14) with Eq. (15) into Eq. (22) and inverting the order of integration and summation, we obtain

$$\tilde{u}_0(\mathbf{k}_t) = \sum_N a_N \tilde{\psi}_N(\mathbf{k}_t), \quad (23)$$

where $\tilde{\psi}_N$ is given in Eq. (21).

By applying the convolution theorem to Eq. (16), we may evaluate the expansion coefficients a_N directly from the *plane-wave spectral* distribution, $\tilde{u}_0(\mathbf{k}_t)$, via

$$a_N = \frac{1}{(2\pi)^2} \int d^2 k_t \tilde{u}_0(\mathbf{k}_t) \tilde{\varphi}_N^*(\mathbf{k}_t), \quad (24)$$

where

$$\tilde{\varphi}_N(\mathbf{k}_t) = \tilde{\varphi}(\mathbf{k}_t - \bar{\mathbf{k}}_t) \exp(j\bar{\mathbf{k}}_t \cdot \bar{\mathbf{r}}_t), \quad (25)$$

is the plane-wave spectrum of $\varphi_N(\mathbf{r}_t)$.

4. VECTORIAL EM FIELD DECOMPOSITION

In order to obtain a TE/TM frame-based representation of the electric field, $\mathbf{E}(\mathbf{r}, t)$, we introduce the TE/TM coefficients

$$\begin{aligned} a_N^{\text{TE}} &= \frac{1}{(2\pi)^2} \int d^2 k_t k_t^{-1} \tilde{E}^{\text{TE}}(\mathbf{k}_t) \tilde{\varphi}_N^*(\mathbf{k}_t), \\ a_N^{\text{TM}} &= \frac{1}{(2\pi)^2} \int d^2 k_t k_t^{-1} \tilde{E}^{\text{TM}}(\mathbf{k}_t) \tilde{\varphi}_N^*(\mathbf{k}_t), \end{aligned} \quad (26)$$

where $\tilde{\varphi}_N(\mathbf{k}_t)$ is given in Eq. (25) and the spectral distributions, \tilde{E}^{TE} and \tilde{E}^{TM} , are given in Eq. (9). The motivation to introduce the k_t^{-1} term in Eq. (26) is discussed after Eq. (32). Thus, by using Eq. (23) for each TE/TM electric field spectral component, we may write

$$\begin{aligned}\tilde{E}^{\text{TE}}(\mathbf{k}_t) &= \sum_N a_N^{\text{TE}} k_t \tilde{\psi}_N(\mathbf{k}_t), \\ \tilde{E}^{\text{TM}}(\mathbf{k}_t) &= \sum_N a_N^{\text{TM}} k_t \tilde{\psi}_N(\mathbf{k}_t),\end{aligned}\quad (27)$$

where $\tilde{\psi}_N(\mathbf{k}_t)$ is given in Eq. (21). By inserting Eq. (27) into Eq. (11) and inverting the order of integration and summation, we obtain, for each field component in Eq. (10),

$$\begin{aligned}\mathbf{E}^{\text{TE}}(\mathbf{r}, t) &= \sum_N a_N^{\text{TE}} \mathbf{E}_N^{\text{TE}}(\mathbf{r}, t), \\ \mathbf{E}^{\text{TM}}(\mathbf{r}, t) &= \sum_N a_N^{\text{TM}} \mathbf{E}_N^{\text{TM}}(\mathbf{r}, t),\end{aligned}\quad (28)$$

where

$$\begin{aligned}\mathbf{E}_N^{\text{TE}}(\mathbf{r}, t) &= \frac{1}{(2\pi)^2} \int d^2 k_t k_t \hat{\mathbf{n}}(\mathbf{k}_t) \tilde{\psi}_N(\mathbf{k}_t) \exp(-j\mathbf{k} \cdot \mathbf{r}), \\ \mathbf{E}_N^{\text{TM}}(\mathbf{r}, t) &= \frac{1}{(2\pi)^2} \int d^2 k_t k_t \hat{\mathbf{t}}(\mathbf{k}_t) \tilde{\psi}_N(\mathbf{k}_t) \exp(-j\mathbf{k} \cdot \mathbf{r}),\end{aligned}\quad (29)$$

are the electric field *TE/TM beam propagators* over the frame lattice. Assuming that $\psi(\mathbf{r}_t)$ is wide on a wavelength scale, the spatial and spectral distributions of ψ_N are localized around the lattice point $\mathbf{r}_t = \bar{\mathbf{r}}_t$ and $\mathbf{k}_t = \bar{\mathbf{k}}_t$, respectively. Consequently, \mathbf{E}_N^{TE} and \mathbf{E}_N^{TM} are collimated EM beams whose axes emerge from a processing-dependent point $\mathbf{r}_t = \bar{\mathbf{r}}_t$ over the $z = 0$ plane, in a processing-dependent direction:

$$\hat{\mathbf{k}} = (\bar{\mathbf{k}}_t, \bar{k}_z)/k, \quad \bar{k}_z = \sqrt{k^2 - \bar{k}_t^2}, \quad (30)$$

where $\bar{k}_t = \sqrt{\bar{k}_x^2 + \bar{k}_y^2}$. Propagating beams occur for $\bar{k}_t < k - \Delta_{k_t}$, where Δ_{k_t} denotes the (plane-wave) spectral width of $\tilde{\psi}(\mathbf{k}_t)$. For $\bar{k}_t > k + \Delta_{k_t}$, the spectral distribution is localized in the evanescent spectral range, and the corresponding beam propagators decay exponentially with z .

The vectorial propagation formulation in Eq. (29) can be reduced to a scalar one in the following manner: by inserting $\hat{\mathbf{n}}$ and $\hat{\mathbf{t}}$ in Eq. (7) into Eq. (29), we obtain

$$\begin{aligned}\mathbf{E}_N^{\text{TE}}(\mathbf{r}, t) &= \frac{1}{(2\pi)^2} \int d^2 k_t (k_y \hat{\mathbf{x}} - k_x \hat{\mathbf{y}}) \tilde{\psi}_N(\mathbf{k}_t) \exp(-j\mathbf{k} \cdot \mathbf{r}), \\ \mathbf{E}_N^{\text{TM}}(\mathbf{r}, t) &= \frac{1}{k(2\pi)^2} \int d^2 k_t [k_z (k_x \hat{\mathbf{x}} + k_y \hat{\mathbf{y}}) - k_t^2 \hat{\mathbf{z}}] \tilde{\psi}_N(\mathbf{k}_t) \\ &\quad \times \exp(-j\mathbf{k} \cdot \mathbf{r}).\end{aligned}\quad (31)$$

Next, by using $k_x \exp(-j\mathbf{k} \cdot \mathbf{r}) = j \frac{\partial}{\partial x} \exp(-j\mathbf{k} \cdot \mathbf{r})$, and so forth, we rewrite Eq. (31) in the form

$$\begin{aligned}\mathbf{E}_N^{\text{TE}}(\mathbf{r}, t) &= j(\hat{x}\partial_y - \hat{y}\partial_x)P_N(\mathbf{r}, t), \\ \mathbf{E}_N^{\text{TM}}(\mathbf{r}, t) &= -k^{-1}(\hat{x}\partial_x\partial_z + \hat{y}\partial_y\partial_z - \hat{z}\nabla_t^2)P_N(\mathbf{r}, t),\end{aligned}\quad (32)$$

where the *scalar beam propagators*, $P_N(\mathbf{r}, t)$, are given in Eq. (20). In Eq. (32) we denote $\partial_x = \partial/\partial x$, $\partial_x^2 = \partial^2/\partial x^2$,

$\nabla_t^2 = \partial_x^2 + \partial_y^2$, and so forth. Note that applying the *differential operators* in Eq. (32) was made possible due to the introduction of the k_t^{-1} term in Eq. (26).

Equations (10), (28), (32), and (20) represent the electric field, $\mathbf{E}(\mathbf{r}, t)$, as a discrete superposition of EM beam-type wave objects, \mathbf{E}_N^{TE} and \mathbf{E}_N^{TM} , which are the TE and TM electric field propagators. The excitation amplitudes of these EM wave objects are obtained from the aperture field spectral distribution, $\tilde{\mathbf{E}}_0$, via Eq. (26). The beam propagators are characterized by transversal localization and high directivity (see specific example for Gaussian windows in Section 5). The representation in Eq. (32) reduces the full vectorial formulation to a scalar one, in which the vector fields are obtained directly from the scalar beam propagators, $P_N(\mathbf{r}, t)$ in Eq. (20).

The magnetic field in $z \geq 0$ can be obtained by applying Faraday's law, $\mathbf{H} = (-j\omega\mu_0)^{-1} \nabla \times \mathbf{E}$, to Eq. (28) and inserting Eq. (32). Thus,

$$\mathbf{H}(\mathbf{r}, t) = \mathbf{H}^{\text{TE}}(\mathbf{r}, t) + \mathbf{H}^{\text{TM}}(\mathbf{r}, t), \quad (33)$$

with

$$\begin{aligned}\mathbf{H}^{\text{TE}}(\mathbf{r}, t) &= \sum_N a_N^{\text{TE}} \mathbf{H}_N^{\text{TE}}(\mathbf{r}, t), \\ \mathbf{H}^{\text{TM}}(\mathbf{r}, t) &= \sum_N a_N^{\text{TM}} \mathbf{H}_N^{\text{TM}}(\mathbf{r}, t),\end{aligned}\quad (34)$$

where a_N^{TE} and a_N^{TM} are given in Eq. (26) and \mathbf{H}_N^{TE} and \mathbf{H}_N^{TM} denote the magnetic fields of the TE and TM EM beam propagators, which can be evaluated from the *scalar beam propagator* $P_N(\mathbf{r}, t)$ in Eq. (20), via

$$\begin{aligned}\mathbf{H}_N^{\text{TE}}(\mathbf{r}, t) &= \frac{-1}{k\eta_0} (\hat{x}\partial_x\partial_z + \hat{y}\partial_y\partial_z - \hat{z}\nabla_t^2)P_N(\mathbf{r}, t), \\ \mathbf{H}_N^{\text{TM}}(\mathbf{r}, t) &= \frac{-1}{j\eta_0} (\hat{x}\partial_y - \hat{y}\partial_x)P_N(\mathbf{r}, t),\end{aligned}\quad (35)$$

where $\eta_0 = \sqrt{\mu_0/\epsilon_0}$ is the (vacuum) wave impedance. In deriving Eq. (35), we have used $\nabla^2 P_N = -k^2 P_N$, which follows from Helmholtz equation (19). Note that the z component is canceled out in the TM magnetic field propagator.

Alternatively, plane-wave spectral representations for \mathbf{H} -fields, similar to the one in Eq. (29), may be practical for asymptotically evaluating these fields in the high-frequency regime. Such representations are obtained by applying the well-known plane-wave spectral relation, $\hat{\mathbf{H}} = \eta_0^{-1} \hat{\mathbf{k}} \times \hat{\mathbf{E}}$, to Eq. (29), which results in

$$\begin{aligned}\mathbf{H}_N^{\text{TE}}(\mathbf{r}, t) &= \frac{1}{\eta_0} \frac{1}{(2\pi)^2} \int d^2 k_t k_t \hat{\mathbf{t}}(\mathbf{k}_t) \tilde{\psi}_N(\mathbf{k}_t) \exp(-j\mathbf{k} \cdot \mathbf{r}), \\ \mathbf{H}_N^{\text{TM}}(\mathbf{r}, t) &= \frac{-1}{\eta_0} \frac{1}{(2\pi)^2} \int d^2 k_t k_t \hat{\mathbf{n}}(\mathbf{k}_t) \tilde{\psi}_N(\mathbf{k}_t) \exp(-j\mathbf{k} \cdot \mathbf{r}),\end{aligned}\quad (36)$$

where the spectral unit vectors, $\hat{\mathbf{n}}$ and $\hat{\mathbf{t}}$, are given in Eq. (7), and $\tilde{\psi}_N$ is the synthesis set spectral distribution in Eq. (21).

5. GAUSSIAN FRAMES AND ASYMPTOTIC EVALUATION

The general frame representation in Eq. (28) is applied here for the special case of Gaussian frames, which have been used extensively for modeling beam propagation because they maximize the localization as implied by the uncertainty

principle and yield analytically trackable beam-type propagators [1,2,4–7,9,10,15,16]. The Gaussian synthesis windows are defined as

$$\psi(\mathbf{r}_t) = \exp(-jk\Gamma r_t^2/2), \quad (37)$$

where $r_t^2 = x^2 + y^2$ and $\Gamma = \Gamma_r + j\Gamma_j$ is the window complex frequency-independent parameter with $\Gamma_j < 0$. By applying the Fourier operator in Eqs. (22)–(37), we obtain the plane-wave spectral distribution of these windows:

$$\tilde{\psi}(\mathbf{k}_t) = -2\pi j(k\Gamma)^{-1} \exp[jk_t^2/(2k\Gamma)]. \quad (38)$$

In order to evaluate the corresponding Gaussian analysis window, we shall make use of the high-oversampling approximation:

$$\varphi(\mathbf{r}_t) \cong \nu_x \nu_y \|\psi\|^{-2} \psi(\mathbf{r}_t), \quad (39)$$

which, for Gaussian windows, is valid for $\nu_{x,y} < 0.4$ (further details are given in [4]). Thus, by inserting $\|\psi\|^2 = -\pi/(k\Gamma_j)$ into Eq. (39), we may approximate the corresponding Gaussian analysis window by

$$\varphi(\mathbf{r}_t) = (-\nu^2 k\Gamma_j/\pi) \exp(-jk\Gamma r_t^2/2), \quad (40)$$

and its plane-wave spectral distribution by

$$\tilde{\varphi}(\mathbf{k}_t) = j2\nu^2 \Gamma_j (\Gamma)^{-1} \exp[jk_t^2/(2k\Gamma)], \quad (41)$$

where $\nu = \nu_x = \nu_y$ is the overcompleteness parameter in Eq. (13). This type of windows gives rise to Gaussian beams that exhibit frequency-independent collimation (Rayleigh) lengths [see Eq. (49)] and, therefore, have been termed isodiffracting [37]. The isodiffracting feature makes these wave objects highly suitable for ultrawideband representations [2,4,10,38–40].

The scalar Gaussian beam propagators, $P_N(\mathbf{r}, t)$, are obtained by inserting Eq. (38) into Eq. (20). The resulting plane-wave spectral integral can be evaluated asymptotically (see details in Appendix A). The paraxial asymptotic scalar Gaussian beam propagators are obtained by utilizing the local beam coordinates, $\mathbf{r}_b = (x_b, y_b, z_b)$, which are defined, for a given spectral point $(\bar{x}, \bar{y}, \bar{k}_x, \bar{k}_y)$ on the frame lattice, by the rotation transformation:

$$\begin{bmatrix} x_b \\ y_b \\ z_b \end{bmatrix} = \begin{bmatrix} \cos \bar{\theta} \cos \bar{\phi} & \cos \bar{\theta} \sin \bar{\phi} & -\sin \bar{\theta} \\ -\sin \bar{\phi} & \cos \bar{\phi} & 0 \\ \sin \bar{\theta} \cos \bar{\phi} & \sin \bar{\theta} \sin \bar{\phi} & \cos \bar{\theta} \end{bmatrix} \begin{bmatrix} x - \bar{x}_x \\ y - \bar{x}_y \\ z \end{bmatrix}, \quad (42)$$

where $(\bar{\theta}, \bar{\phi})$ are the spherical angles that define the spectral unit vector $\hat{\mathbf{k}}$ in Eq. (30), i.e.,

$$\cos \bar{\theta} = \bar{k}_z/k, \quad \cos \bar{\phi} = \bar{k}_x/\bar{k}_t, \quad \sin \bar{\phi} = \bar{k}_y/\bar{k}_t. \quad (43)$$

Thus, *on-axis* observation points, for which (see Fig. 2)

$$\mathbf{r}_t - \bar{\mathbf{r}}_t = z \tan \bar{\theta} (\cos \bar{\phi} \hat{\mathbf{x}} + \sin \bar{\phi} \hat{\mathbf{y}}), \quad (44)$$

are identified by $x_b = y_b = 0$. By utilizing the beam coordinates, the beam propagators are evaluated asymptotically as (see details in Appendix A)

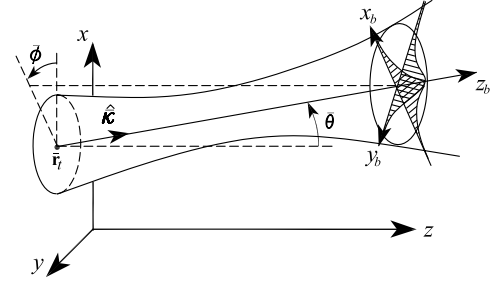


Fig. 2. Local beam coordinates. The asymptotic Gaussian beam propagator is described in terms of the local beam-coordinates, $\mathbf{r}_b = (x_b, y_b, z_b)$, which are defined in Eq. (42). The beam propagates along the z_b axis and exhibits a Gaussian decay in the transverse coordinates x_b and y_b .

$$P_N(\mathbf{r}, t) \sim \sqrt{\frac{\Gamma_x(z_b)}{\Gamma_x(0)}} \sqrt{\frac{\Gamma_y(z_b)}{\Gamma_y(0)}} \exp[-jk\Psi(\mathbf{r}_b)], \quad (45)$$

$$\Psi(\mathbf{r}_b) = z_b + \frac{1}{2} [\Gamma_x(z_b)x_b^2 + \Gamma_y(z_b)y_b^2],$$

where

$$\Gamma_x(z_b) = 1/(z_b + \cos^2 \bar{\theta} \Gamma^{-1}), \quad \Gamma_y(z_b) = 1/(z_b + \Gamma^{-1}), \quad (46)$$

are the so-called complex curvatures of the Gaussian beam.

In order to parameterize the Gaussian beam propagator, we denote the real and the imaginary part of $1/\Gamma$ by $-Z$ and F , respectively, i.e.,

$$\Gamma^{-1} = -Z + jF. \quad (47)$$

Thus, the complex curvatures in Eq. (46) can be recast in the form

$$\Gamma_{x,y}(z_b) = 1/(z_b - Z_{x,y} + jF_{x,y}), \quad (48)$$

where

$$Z_x = Z \cos^2 \bar{\theta}, \quad Z_y = Z, \quad F_x = F \cos^2 \bar{\theta}, \quad F_y = F. \quad (49)$$

By using Eq. (48) in Eq. (45), one finds that the Gaussian beam exhibits (pure) quadratic decay in the (x_b, y_b) directions with corresponding e^{-1} beam widths of

$$W_{x,y}(z_b) = D_{x,y} \sqrt{1 + \frac{(z_b - Z_{x,y})^2}{F_{x,y}^2}}, \quad (50)$$

where $D_{x,y} = \sqrt{8F_{x,y}}/k$ are identified as the principal beam widths at the waists. By using Eq. (50), we identify $F_{x,y}$ as the beam collimation lengths and $Z_{x,y}$ is identified as the beam waist locations on the (x_b, z_b) and (y_b, z_b) principal planes. The beam field remains collimated near the waist where $|z_b - Z_{x,y}| \ll F_{x,y}$, whereas, away from the waists, it opens up along constant diffraction angles of $\Theta_{x,y} = (kF_{x,y}/8)^{-1/2}$. Finally, by taking the real part of the complex curvatures in Eq. (46), we find that the principal phase-front radii of curvature in the (x_b, z_b) and (y_b, z_b) planes, $R_{x,y}$, are given by

$$R_{x,y} = (z_b - Z_{x,y}) + F_{x,y}^2/(z_b - Z_{x,y}). \quad (51)$$

The *electric field* Gaussian propagators are evaluated asymptotically by inserting Eq. (45) into Eq. (32) and collecting the highest asymptotic (k -) order (note, that according to Eq. (45), the transverse coordinates, x_b and y_b , are of the order of $1/\sqrt{k}$ [15]). Alternatively, these propagators can be evaluated directly from their plane-wave spectral representations in Eq. (29). Note that the electric field spectral integrals in Eq. (29) and the scalar field representation in Eq. (20) differ only in the *amplitude* functions, which, in the asymptotic procedure, are sampled at the *on-axis* stationary point $(k_x, k_y) = (\bar{k}_x, \bar{k}_y)$. Thus, by using Eq. (38) in Eq. (21) and inserting into Eq. (29), the asymptotic electric field TE propagators, \mathbf{E}_N^{TE} , are evaluated asymptotically by

$$\mathbf{E}_N^{\text{TE}}(\mathbf{r}, t) \sim \bar{k}_t \hat{\mathbf{n}}(\bar{\mathbf{k}}_t) P_N(\mathbf{r}, t), \quad (52)$$

where $P_N(\mathbf{r}, t)$ is given in Eq. (45), and $\hat{\mathbf{n}}(\bar{\mathbf{k}}_t) = \hat{\mathbf{n}}|_{\mathbf{k}_t=\bar{\mathbf{k}}_t}$ is defined in Eq. (7). By applying the same procedure to the spectral integral in Eq. (36), we obtain the corresponding magnetic field

$$\mathbf{H}_N^{\text{TE}}(\mathbf{r}, t) \sim \frac{1}{\eta_0} \bar{k}_t \hat{\mathbf{t}}(\bar{\mathbf{k}}_t) P_N(\mathbf{r}, t). \quad (53)$$

The TM field propagators, \mathbf{E}_N^{TM} and \mathbf{H}_N^{TM} , are obtained in a similar manner from Eqs. (29) and (36), yielding

$$\mathbf{E}_N^{\text{TM}}(\mathbf{r}, t) \sim \bar{k}_t \hat{\mathbf{t}}(\bar{\mathbf{k}}_t) P_N(\mathbf{r}, t), \quad \mathbf{H}_N^{\text{TM}}(\mathbf{r}, t) \sim \eta_0^{-1} \bar{k}_t \hat{\mathbf{n}}(\bar{\mathbf{k}}_t) P_N(\mathbf{r}, t). \quad (54)$$

Equations (52)–(54) describe the asymptotic TE and TM EM Gaussian beam propagators corresponding to the Gaussian synthesis window in Eq. (37) in terms of the scalar beam propagators in Eq. (45).

6. NUMERICAL EXAMPLE

A. Scalar Formulation

This section demonstrates the implementation of the scalar beam summation process. The reference field is a complex source beam field of the form

$$u(\mathbf{r}) = \frac{A}{kR} \exp(-jkR), \quad R = \sqrt{(x-x')^2 + (y-y')^2 + (z-z')^2}, \quad (55)$$

where A is some constant and the source location, $\mathbf{r}' = (x', y', z')$ carries a complex shift, which is taken in this example to be $\mathbf{r}' = \lambda(2j, 2j, -2 + 10j)$, where λ denotes the wavelength. The resulting beam field source disk is centered at $z = -2\lambda$ and the beam propagated in a direction of the unit vector $\hat{\mathbf{k}}_b = (1, 1, 5)/\sqrt{27}$. The aperture field is obtained by sampling $u(\mathbf{r}, t)$ in Eq. (55) over a $10\lambda \times 10\lambda$ square in the $z = 0$ plane.

The processing (analysis) window is given by Eq. (37) with $\Gamma = (0.013 - 0.32j)/\lambda$. This choice results in a Gaussian window with e^{-1} width of 1λ and beam waist location of $z = 5\lambda$. The overcompleteness parameter is $\nu = 0.5$ and, accordingly, $\Delta \bar{x} = \sqrt{2}/2\lambda$ and $\Delta \bar{k}_x/k = \sqrt{2}/4$. The coefficients were evaluated for $|\bar{x}| \leq 15\lambda$ and $|\bar{k}_{x,y}| \leq k$ (only propagating spectrum components are included).

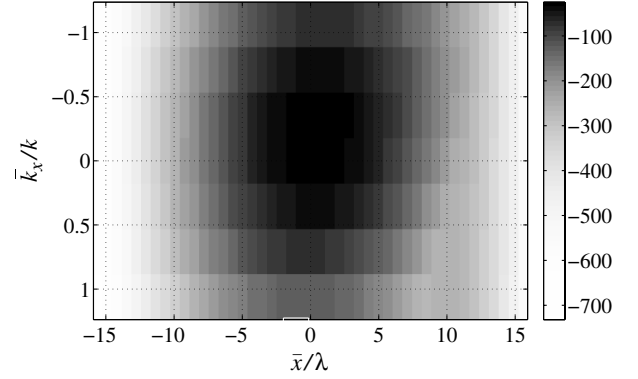


Fig. 3. Coefficients map for $u_0(\mathbf{r}_t)$ over the (\bar{k}_x, \bar{x}) plane.

The absolute value of resulting a_N coefficients $45 \times 45 \times 5 \times 5$ array is plotted for $\bar{y} = 0$, $\bar{k}_y = 0$ in Fig. 3. The \bar{k}_x axis was normalized with respect to the wavenumber k . Note that most of the spectrum is located in the propagating $|\bar{k}_x| < k$ region. The evanescent spectrum was excluded from the reconstructed field.

The field was reconstructed as a summation of Gaussian beams of the form in Eq. (18) with Eq. (45) over the $z = 7\lambda$ plane. The resulting scalar field is plotted in Fig. 4. The real part of the reference analytic solution in Eq. (55) is plotted in Fig. 4(a) and the frame-based summation solution in Fig. 4(b). In order to compare the reference field in Eq. (55) with the reconstructed one in Eq. (18), the absolute values of the difference of their real and imaginary parts are plotted in Figs. 5(a) and 5(b) respectively. The figures show that the error is less than -62 dB from the reference field maximum.

B. EM Formulation

In this subsection we evaluate numerically the EM field using the TE/TM decomposition in Section 4. We process the aperture field distribution $\mathbf{E}_0(\mathbf{r}_t) = E_x(\mathbf{r}_t)\hat{\mathbf{x}}$, where E_x is the scalar distribution in Eq. (55). The processing (analysis) window is given by Eq. (37). The expansion parameters are all as in Subsection 6.A.

The absolute value of the a_N^{TE} and a_N^{TM} coefficients $45 \times 45 \times 5 \times 5$ arrays are plotted for $\bar{y} = 0$, $\bar{k}_y = 0$ in Fig. 6. The TE and TM electric fields were reconstructed as a summation of the form in Eq. (28) over the TE/TM Gaussian beam propagators in Eqs. (52)–(54) over the $z = 7\lambda$ plane. In order to compare the resulting fields with the reference analytic solution in Eq. (55), we sum the x components of \mathbf{E}^{TE} and \mathbf{E}^{TM} . The absolute values of the difference of the real and imaginary parts of the resulting E_x field and the reference field in decibels are plotted in Figs. 7(a) and 7(b), respectively. The figure shows that the error is less than -50 dB from the reference field maximum. Note that the accuracy of the TE/TM expansion is about -12 dB of the scalar representation in Subsection 6.A. This reduction in the accuracy is due to the vectorial processing, which involves an additional computation effort. The accuracy can be enhanced by applying a denser spectral grid. For the specific example, by using $\nu = 0.25$, the maximum error reduces to -61 dB.

7. SUMMARY

Application of an exact beam-type expansion to EM waves was introduced, in which the basic building block waveobjects,

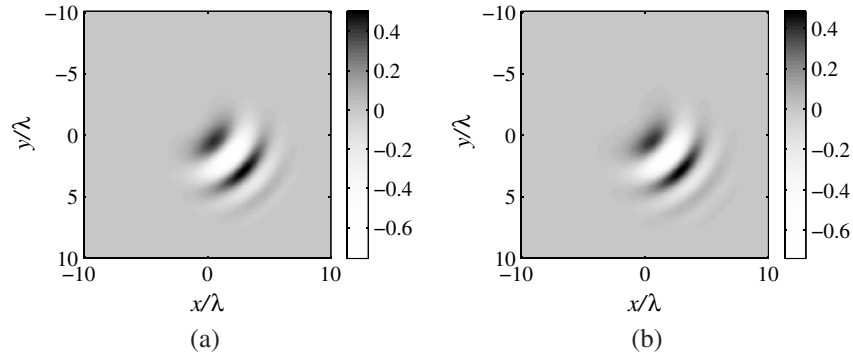


Fig. 4. Real part of the (a) reference and (b) reconstructed scalar field over the $z = 7\lambda$ plane.

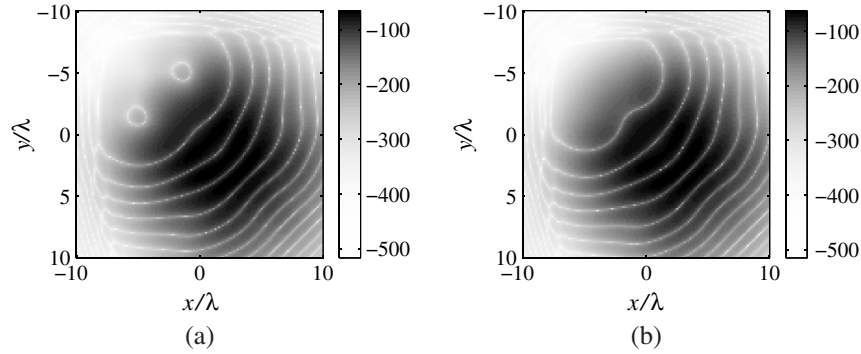


Fig. 5. Error of reconstructed field over the $z = 7\lambda$ plane with respect to the reference field in decibels from the maximum value of the reference field for (a) the real part and (b) the imaginary part. The errors do not exceed -62 dB error.

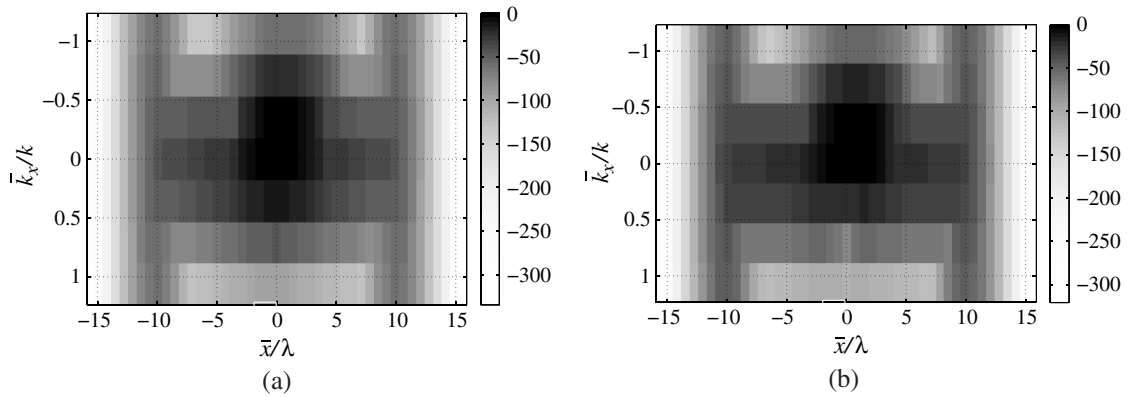


Fig. 6. Coefficients map for $E_0(\mathbf{r}_t)$ over the (\bar{k}_x, \bar{x}) plane for (a) TE coefficients and (b) TM coefficients.

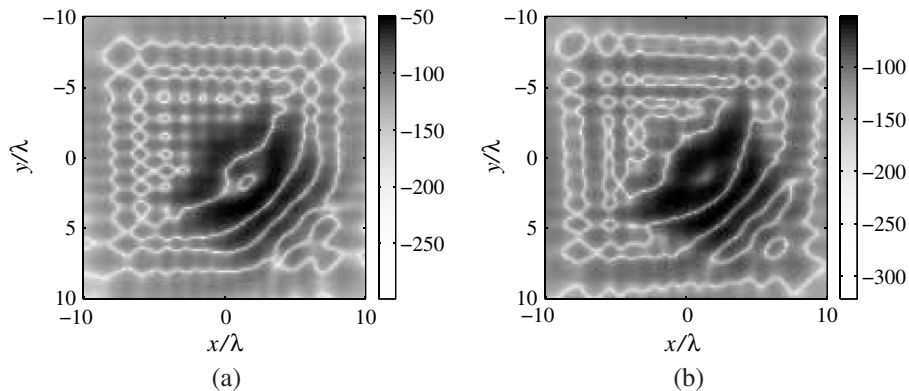


Fig. 7. Error of reconstructed E_x field over the $z = 7\lambda$ plane with respect to the reference field in decibels from the maximum value of the reference field for (a) the real part and (b) the imaginary part. The errors do not exceed -50 dB error.

the EM Gaussian beams, were decomposed into TE and TM fields with respect to constant z planes. This procedure is essential for applying Maxwell's boundary conditions for solving different scattering problems. In Eqs. (28) and (34), the propagating EM field is described as a discrete superposition of the TE and TM EM beam propagators in Eqs. (29) and (36), which are shifted and tilted to points and directions according to the frame spatial-directional lattice in Eq. (12). These *vector* wave objects can be obtained from the *scalar* propagator in Eq. (20) via the differential operators in Eqs. (32) and (35). Explicit asymptotic expressions for the scalar Gaussian beam propagators, P_N , as well as for the EM ones, were obtained in Eqs. (45) and (52)–(54).

APPENDIX A: ASYMPTOTIC EVALUATION OF EQ. (20)

In order to asymptotically evaluate the scalar Gaussian beam propagator, we express Eq. (20) with Eq. (21) for spectral window (38), in the form

$$P_N(\mathbf{r}, t) = (2\pi j k \Gamma)^{-1} \int d^2 k_t \exp[-j q(\mathbf{k}_t)],$$

$$q(\mathbf{k}_t) = \mathbf{k}_t^T (\mathbf{r}_t - \bar{\mathbf{r}}_t) + k_z z - (2k\Gamma)^{-1} (\mathbf{k}_t - \bar{\mathbf{k}}_t)^T (\mathbf{k}_t - \bar{\mathbf{k}}_t), \quad (\text{A.1})$$

where, here and henceforth, all vectors are assumed to be column vectors and superscript T denotes vector or matrix transpose. Integral (A.1) has a stationary point \mathbf{k}_{t_s} in the complex \mathbf{k}_t domain, which is defined by

$$\nabla_{\mathbf{k}_t} q = \mathbf{r}_t - \bar{\mathbf{r}}_t - \mathbf{k}_{t_s} z / k_{z_s} - (k\Gamma)^{-1} (\mathbf{k}_{t_s} - \bar{\mathbf{k}}_t) = 0, \quad (\text{A.2})$$

where $k_{z_s} = \sqrt{k^2 - \mathbf{k}_{t_s}^T \mathbf{k}_{t_s}}$. Note that, for an *on-axis* observation point, where $\bar{\mathbf{k}}_z(\mathbf{r}_t - \bar{\mathbf{r}}_t) = \bar{\mathbf{k}}_t z$ [see Eq. (44)], this equation has a real solution, $\mathbf{k}_{t_s} = \bar{\mathbf{k}}_t$. For off-axis observation points, the solution of Eq. (A.2) is complex and cannot be found explicitly. However, the stationary point can be approximated for observation points near the beam axis, by expanding $q(\mathbf{k}_t)$ into a Taylor series about the on-axis stationary point $\bar{\mathbf{k}}_t$, i.e.,

$$q(\mathbf{k}_t) = q_0 + \mathbf{q}_1^T (\mathbf{k}_t - \bar{\mathbf{k}}_t) + \frac{1}{2} (\mathbf{k}_t - \bar{\mathbf{k}}_t)^T \mathbf{q}_2 (\mathbf{k}_t - \bar{\mathbf{k}}_t), \quad (\text{A.3})$$

with the coefficients

$$q_0 = \bar{\mathbf{k}}_t^T (\mathbf{r}_t - \bar{\mathbf{r}}_t) + \bar{k}_z z, \quad \mathbf{q}_1 = \mathbf{r}_t - \bar{\mathbf{r}}_t - z \bar{\mathbf{k}}_t / k_z, \quad (\text{A.4})$$

and

$$\mathbf{q}_2 = - \begin{bmatrix} \frac{1}{k\Gamma} + \frac{z(\bar{k}_x^2 + \bar{k}_y^2)}{k_z^3} & \frac{z\bar{k}_x \bar{k}_y}{k_z^3} \\ \frac{z\bar{k}_x \bar{k}_y}{k_z^3} & \frac{1}{k\Gamma} + \frac{z(\bar{k}_y^2 + \bar{k}_x^2)}{k_z^3} \end{bmatrix}. \quad (\text{A.5})$$

By using Eq. (A.3), the stationary point is approximated by

$$\mathbf{k}_{t_s} = \bar{\mathbf{k}}_t - \mathbf{q}_2^{-1} \mathbf{q}_1, \quad (\text{A.6})$$

and the scalar propagator, $P_N(\mathbf{r}, t)$, may be asymptotically approximated over the SDP path via [41]

$$P_N(\mathbf{r}, t) \sim \frac{(k\Gamma)^{-1}}{\sqrt{\det \mathbf{q}_2}} \exp \left[-j \left(q_0 - \frac{1}{2} \mathbf{q}_1^T \mathbf{q}_2^{-1} \mathbf{q}_1 \right) \right]. \quad (\text{A.7})$$

Next, by utilizing the beam-coordinates in Eq. (42), we may evaluate the Taylor coefficients, $q_0 = k z_b$:

$$\mathbf{q}_1 = \begin{bmatrix} \cos \bar{\phi} / \cos \bar{\theta} & -\sin \bar{\phi} \\ \sin \bar{\phi} / \cos \bar{\theta} & \cos \bar{\phi} \end{bmatrix} \begin{bmatrix} x_b \\ y_b \end{bmatrix}, \quad (\text{A.8})$$

and, thus,

$$-\mathbf{q}_1^T \mathbf{q}_2^{-1} \mathbf{q}_1 = x_b^2 \Gamma_x(z) + y_b^2 \Gamma_y(z), \quad (\text{A.9})$$

with

$$\Gamma_x(z) = (z / \cos \bar{\theta} + \cos^2 \bar{\theta} \Gamma^{-1})^{-1},$$

$$\Gamma_y(z) = (z / \cos \bar{\theta} + \Gamma^{-1})^{-1}. \quad (\text{A.10})$$

Finally, the conventional (paraxial) Gaussian beams are obtained by applying the small-angle approximation. By using Eq. (42), we can substitute $z / \cos \bar{\theta} = z_b - x_{b1} \tan \bar{\theta} \simeq z_b$ into Eq. (A.10), and obtain the final result in Eq. (46). By using Eq. (A.8) in Eq. (A.6), we note that the displacement of the stationary point, \mathbf{k}_{t_s} , from the corresponding on-axis real value, $\bar{\mathbf{k}}_t$, is proportional to $[x_b, y_b]$, thereby justifying the Taylor analysis for observation points with small transverse deviation from the beam axis.

REFERENCES

1. B. Steinberg, E. Heyman, and L. Felsen, "Phase space beam summation for time-harmonic radiation from large apertures," *J. Opt. Soc. Am. A* **8**, 41–59 (1991).
2. T. Melamed, "Phase-space beam summation: a local spectrum analysis for time-dependent radiation," *J. Electromagn. Waves Appl.* **11**, 739–773 (1997).
3. J. M. Arnold, "Rays, beams and diffraction in a discrete phase space: Wilson bases," *Opt. Express* **10**, 716–727 (2002).
4. A. Shlivinski, E. Heyman, A. Boag, and C. Letrou, "A phase-space beam summation formulation for ultra wideband radiation," *IEEE Trans. Antennas Propag.* **52**, 2042–2056 (2004).
5. G. Gordon, E. Heyman, and R. Mazar, "A phase-space Gaussian beam summation representation of rough surface scattering," *J. Acoust. Soc. Am.* **117**, 1911–1921 (2005).
6. M. Katsav and E. Heyman, "Phase space Gaussian beam summation analysis of half plane diffraction," *IEEE Trans. Antennas Propag.* **55**, 1535–1545 (2007).
7. T. Melamed, "Phase-space Green's functions for modeling time-harmonic scattering from smooth inhomogeneous objects," *J. Math. Phys.* **45**, 2232–2246 (2004).
8. T. Melamed, "Time-domain phase-space Green's functions for inhomogeneous media," in *Ultrawideband/Short Pulse Electromagnetics 6*, E. L. Mokole, M. Kragalott, K. R. Gerlach, M. Kragalott, and K. R. Gerlach, ed. (Springer-Verlag, 2007), pp. 56–63.
9. I. Tinkelman and T. Melamed, "Gaussian beam propagation in generic anisotropic wavenumber profiles," *Opt. Lett.* **28**, 1081–1083 (2003).
10. I. Tinkelman and T. Melamed, "Local spectrum analysis of field propagation in an anisotropic medium. Part I. Time-harmonic fields," *J. Opt. Soc. Am. A* **22**, 1200–1207 (2005).
11. I. Tinkelman and T. Melamed, "Local spectrum analysis of field propagation in an anisotropic medium. Part II. Time-dependent fields," *J. Opt. Soc. Am. A* **22**, 1208–1215 (2005).
12. T. Melamed and L. Felsen, "Pulsed beam propagation in lossless dispersive media. Part I. Theory," *J. Opt. Soc. Am. A* **15**, 1268–1276 (1998).
13. T. Melamed and L. Felsen, "Pulsed beam propagation in lossless dispersive media. Part II. A numerical example," *J. Opt. Soc. Am. A* **15**, 1277–1284 (1998).

14. T. Melamed and L. B. Felsen, "Pulsed beam propagation in dispersive media via pulsed plane wave spectral decomposition," *IEEE Trans. Antennas Propag.* **48**, 901–908 (2000).
15. V. Červený, M. M. Popov, and I. Pšenčík, "Computation of wave fields in inhomogeneous media—Gaussian beam approach," *Geophys. J. R. Astron. Soc.* **70**, 109–128 (1982).
16. B. W. A. N. Norris and J. Schrieffer, "Gaussian wave packets in inhomogeneous media with curved interfaces," *Proc. R. Soc. London Ser. A* **412**, 93–123 (1987).
17. E. Heyman, "Pulsed beam propagation in an inhomogeneous medium," *IEEE Trans. Antennas Propag.* **42**, 311–319 (1994).
18. R. Collin, "Scattering of an incident Gaussian beam by a perfectly conducting rough surface," *IEEE Trans. Antennas Propag.* **42**, 70–4 (1994).
19. O. Kilic and R. Lang, "Scattering of a pulsed beam by a random medium over ground," *J. Electromagn. Waves Appl.* **15**, 481–516 (2001).
20. O. Pascal, F. Lemaitre, and G. Soum, "Paraxial approximation effect on a dielectric interface analysis," *Ann. Telecommun.* **51**, 206–218 (1996).
21. H. Anastassiou and P. Pathak, "Closed form solution for three-dimensional reflection of an arbitrary Gaussian beam by a smooth surface," *Radio Sci.* **37**, 1–8 (2002).
22. J. Hillairet, J. Sokoloff, S. Bolioli, and P. F. Combes, "Analytical physical optics scattering from a PEC finite plate illuminated by a vector Gaussian beam," in *2007 International Conference on Electromagnetics in Advanced Applications* (2007), pp. 170–173.
23. F. Bass and L. Resnick, "Wave beam propagation in layered media," *Prog. Electromagn. Res.* **38**, 111–123 (2002).
24. J. Kong, "Electromagnetic wave interaction with stratified negative isotropic media," *J. Electromagn. Waves Appl.* **15**, 1319–1320 (2001).
25. Y. Hadad and T. Melamed, "Non-orthogonal domain parabolic equation and its Gaussian beam solutions," *IEEE Trans. Antennas Propag.* **58**, 1164–1172 (2010).
26. Y. Hadad and T. Melamed, "Parameterization of the tilted Gaussian beam waveobjects," *Prog. Electromagn. Res. PIER* **102**, 65–80 (2010).
27. Y. Hadad and T. Melamed, "Tilted Gaussian beam propagation in inhomogeneous media," *J. Opt. Soc. Am. A* **27**, 1840–1850 (2010).
28. B. Steinberg and E. Heyman, "Phase space beam summation for time dependent radiation from large apertures: discretized parametrization," *J. Opt. Soc. Am. A* **8**, 959–966 (1991).
29. H.-T. Chou, P. Pathak, and R. Burkholder, "Application of Gaussian-ray basis functions for the rapid analysis of electromagnetic radiation from reflector antennas," *IEE Proc. Microw. Antennas Propag.* **150**, 177–83 (2003).
30. H.-T. Chou, P. Pathak, and R. Burkholder, "Novel Gaussian beam method for the rapid analysis of large reflector antennas," *IEEE Trans. Antennas Propag.* **49**, 880–93 (2001).
31. H.-T. Chou and P. Pathak, "Fast Gaussian beam based synthesis of shaped reflector antennas for contoured beam applications," *IEE Proc. Microw. Antennas Propag.* **151**, 13–20 (2004).
32. T. Melamed, "Exact beam decomposition of time-harmonic electromagnetic waves," *J. Electromagn. Waves Appl.* **23**, 975–986 (2009).
33. R. Martínez-Herrero, P. Mejías, S. Bosch, and A. Carnicer, "Vectorial structure of nonparaxial electromagnetic beams," *J. Opt. Soc. Am. A* **18**, 1678–1680 (2001).
34. H. Guo, J. Chen, and S. Zhuang, "Vector plane wave spectrum of an arbitrary polarized electromagnetic wave," *Opt. Express* **14**, 2095–2100 (2006).
35. D. Gabor, "A new microscopic principle," *Nature* **161**, 777 (1948).
36. J. Wexler and S. Raz, "Discrete Gabor expansions," *Signal Process.* **21**, 207–20 (1990).
37. E. Heyman and T. Melamed, "Certain considerations in aperture synthesis of ultrawideband/short-pulse radiation," *IEEE Trans. Antennas Propag.* **42**, 518–525 (1994).
38. E. Heyman and T. Melamed, *Space-Time Representation of Ultra Wideband Signals* (Elsevier, 1998), pp. 1–63.
39. A. Shlivinski, E. Heyman, and A. Boag, "A phase-space beam summation formulation for ultrawide-band radiation. Part II: A multiband scheme," *IEEE Trans. Antennas Propag.* **53**, 948–957 (2005).
40. A. Shlivinski, E. Heyman, and A. Boag, "A pulsed beam summation formulation for short pulse radiation based on windowed radon transform (WRT) frames," *IEEE Trans. Antennas Propag.* **53**, 3030–3048 (2005).
41. L. Felsen and N. Marcuvitz, *Radiation and Scattering of Waves*, Classic reissue (IEEE, 1994), Chap. 4.2.